Available online at www.sciencedirect.com

ScienceDirect

Proceedings of the Combustion Institute 38 (2021) 6493–6501

Proceedings of the Combustion Institute

www.elsevier.com/locate/proci

Transient behavior and reaction mechanism of CO catalytic ignition over a CuO–CeO_2 mixed oxide

Running Kang [a,b], Pandong Ma [a,c], Junyao He [a], Huixin Li [a], Feng Bin [a,b,d,*], Xiaolin Wei [a,b,d], Baojuan Dou [c], Kwun Nam Hui [e], Kwan San Hui [f,**]

[a] *State Key Laboratory of High-Temperature Gas Dynamics, Institute of Mechanics, Chinese Academy of Sciences, Beijing 100190, PR China*

[b] *School of Engineering Science, University of Chinese Academy of Sciences, 100049 Beijing, PR China*

[c] *Tianjin University of Science & Technology, Tianjin 300457, PR China*

[d] *Dalian National Laboratory for Clean Energy, Dalian 116023, PR China*

[e] *Institute of Applied Physics and Materials Engineering, University of Macau, Avenida da Universidade, Taipa, Macau, PR China*

[f] *Engineering, Faculty of Science, University of East Anglia, Norwich Research Park, NR4 7TJ, United Kingdom*

Received 6 November 2019; accepted 7 June 2020
Available online 25 August 2020

Abstract

This study focuses on the variation in activity-controlling factors during CO catalytic ignition over a CuO–CeO_2 catalyst. The activity for CO combustion follows the decreasing order of CuO–CeO_2 > CuO > CeO_2. Except for inactive CeO_2, increasing temperature induces CO ignition to achieve self-sustained combustion over CuO and CuO–CeO_2. However, CuO provides enough copper sites to adsorb CO, and abundant active lattice oxygen, thus obtaining a higher hot zone temperature (208.3°C) than that of CuO–CeO_2 (197.3 °C). Catalytic ignition triggers a kinetic transition from the low-rate steady-state regime to a high-rate steady-state regime. During the induction process, Raman, X-ray photoelectron spectroscopy (XPS), CO temperature-programmed desorption (CO-TPD) and infrared (IR) spectroscopy results suggested that CO is preferentially adsorbed on oxygen vacancies (Cu^+-[O_v]-Ce^{3+}) to yield Cu^+-[C≡O]-Ce^{3+} complexes. Because of the self-poisoning of CO, the adsorbed CO and traces of adsorbed oxygen react at a relative rate, which is entirely governed by the kinetics on the CO-covered surface and the heat transport until the pre-ignition regime. Nonetheless, the Cu^+-[C≡O]-Ce^{3+} complex is a major contributor to CO ignition. The step-response runs and kinetic models testified that after ignition, a kinetic phase transition occurs from a CO-covered surface to an active lattice oxygen-covered surface. During CO self-sustained combustion, the rapid gas diffusivity

* Corresponding author at: State Key Laboratory of High-Temperature Gas Dynamics, Institute of Mechanics, Chinese Academy of Sciences, Beijing 100190, PR China.

** Corresponding author.

E-mail addresses: binfeng@imech.ac.cn (F. Bin), k.hui@uea.ac.uk (K.S. Hui).

https://doi.org/10.1016/j.proci.2020.06.186

and mass transfer is beneficial for handling the low coverage of CO. The active lattice oxygen of CuO takes part in CO oxidation.

Keywords: Catalytic ignition; Carbon monoxide; Copper-cerium oxide; Transient behavior; Reaction mechanism

1. Introduction

As a key heterogeneous process, the catalytic oxidation of CO is essential not only for practical applications such as automotive exhaust purification and fuel cells but also as a model reaction to study the reaction mechanism and structure-reactivity correlation of catalysts [1]. Our previous studies provided evidence that a high level of CO can be ignited over a catalyst under a $CO/O_2/N_2$ atmosphere. When the catalytic converter warms up to its ignition temperature, the sudden self-acceleration of the surface rate leads to a thermochemical runaway, followed by a rapid transition to self-sustained catalytic combustion [2]. The identified scenario can be applied in the recovery of chemical heat in steelmaking off-gas systems. Because the CO/O_2 mixture tends to cause explosions, the off-gas yielded at steelmaking intermissions is discharged into the atmosphere via CH_4 combustion-supporting flare burners. To recover the chemical heat, self-sustained catalytic combustion can be employed since a catalyst permits the flameless combustion of CO, which avoids the possibility of an explosion. Such a strategy also enables CO burning outside the flammability limits where the combustion can run efficiently at relatively low temperatures, thus simultaneously reducing the formation of NO_x.

Copper-cerium bimetal catalysts have been accepted as an alternative to noble metals due to their considerable activity and durability during CO combustion. However, the relevant active sites over CuO–CeO_2 catalysts remain an unresolved problem. Via acid/base pretreatment to remove dispersed CuO_x or Cu-[O_v]-Ce structures, highly dispersed CuO_x clusters are commonly determined as the active components, whereas ceria, with prominent redox behavior, tunes the dispersion and chemical state of the copper nanoparticles [3]. It has been confirmed that the CuO–CeO_2 exhibits activity via active sites: dispersed CuO_x interacting with ceria > less interacting CuO_x > bulk CuO, and has good resistance towards CO_2 and H_2O [4–6]. The dispersed CuO_x and adjacent oxygen vacancies contribute to the activity, where the Cu^+ are adsorption sites for the chemisorption/activation of CO molecules and the surface reactive oxygen participates directly in the whole CO oxidation process [7,8]. Strongly bound Cu-[O_v]-Ce, which is located at the copper-cerium interface, promotes catalytic activity by providing the sites for CO adsorption [9]. This hypothesis is based on intensive experimental studies on direct (CuO/CeO_2)-inverse (CeO_2/CuO) systems. The interfacial synergy often manifests in unique geometrical, chemical or electronic properties that are complex, even for simple reaction systems. Hence, the experimental verification of the roles played by the copper and cerium ions during CO oxidation requires a specific analysis that is sensitive enough to determine the active states under different reaction conditions.

The catalytic ignition of CO is a complex process that includes kinetics and heat generation since the heat produced is governed by the reaction rate, which in turn is determined by the reaction kinetics. Correspondingly, a transition from low-reactivity steady state to high-reactivity steady state can be observed due to heat transfer limitation, which exhibits different reaction processes. Our previous papers reported that the CO self-combustion passed 200-hour stability test and had the excellent resistance of water [10,11]. Based on the CuO–CeO_2 catalysts, however, current studies of CO oxidation have focused on the reaction mechanism at a low-reactivity state, considering the potential application needs. As an interdisciplinary and promising research topic, this work focuses on the two-step transitions during CO catalytic ignition, and aims to bridge the missing gap between the catalyst and combustion researchers in understanding the fundamental reaction mechanism of CO oxidation over the CuO–CeO_2 catalyst. Specifically, using step-response runs, in situ IR and phase-transition kinetic models etc., this work deepens the understanding of reaction mechanism that CO adsorbed at oxygen vacancies to form Cu^+-[C≡O]-Ce^{3+} species is a major contributor to CO ignition in induction process. More importantly, we revealed that the CuO rather than CeO_2 provides lattice oxygen to participate in the CO self-sustaining catalytic combustion for the first time. This study contributes to a deeper understanding of the reaction mechanism of CO catalytic combustion, expanding from the intrinsic reaction kinetics stage to the self-sustaining catalytic combustion stage, and proposes a CO self-combustion technology to treat the steelmaking off-gas system.

2. Experimental specifications

2.1. Synthesis of the catalysts

$Cu(NO_3)_2$•$3H_2O$ and $Ce(NO_3)_3$•$6H_2O$ were combined in a 1:1 molar ratio and were dissolved fully in 140 mL of ethanol at 80°C. As a pore former, an oxalic acid solution (0.24 mol/L) was added quickly to the aforementioned nitrate solution with stirring to fully dissolve and evaporate ethanol until a gel was formed at 80°C. After aging at room temperature for 48 h, the gel was dried at 105°C for 12 h and then calcined in air at 550°C for 2 h. The catalyst obtained was labeled CuO–CeO_2. To compare the influence of the copper and cerium oxides on CO oxidation, the catalysts, labeled CuO and CeO_2, respectively, were prepared using the same procedure. The Brunauer-Emmett-Teller (BET) surface areas for CuO, CeO_2 and CuO–CeO_2 are 4.3, 66.4 and 44.6 m^2/g, respectively.

2.2. Characterization

X-ray powder diffraction (XRD) patterns were collected on an XD-3-automatic diffractometer (PERSEE) equipped with nickel-filtered Cu Kα radiation. Raman measurements were carried out using a HORIBA LabRAM HR Evolution spectrometer at an excitation laser wavelength of 488 nm. X-ray photoelectron spectroscopy (XPS) was performed using a Kratos Axis Ultra DLD spectrometer. Temperature-programmed reduction (H_2-TPR) was carried out on a TP5080B chemisorption analyzer. Each sample (100 mg) was reduced in a flow of a 5% H_2/He mixture (50 mL/min), with the temperature increasing from room temperature to 700°C at a heating rate of 10°C/min. The temperature-programmed desorption of O_2 and CO (O_2- and CO-TPD-MS) were performed via the same TP5080B instrument, where 5% O_2/He and 5% CO/He mixtures were employed, respectively. O_2 or CO was adsorbed at 50°C for 30 min and then was exposed to He. After the baseline was stable, the reactor was heated at a rate of 10°C/min until reaching 1000°C. TPD spectra were taken with a quadrupole mass spectrometer (Pfeiffer PrismaPlus). In situ IR spectra were recorded on the Bruker Tensor 27 instrument coupled with a self-designed magnetically driven transmission cell, where approximately 20 mg of catalysts was pressed into a self-supporting wafer. Because the optical path can be switched between the gas phase and catalyst by driving a quartz holder outside of the cell, the gas phase signals can be subtracted from the spectra at each tested temperature (Fig. S1 in the supporting information). Prior to recording the spectra, the self-supporting sample disk was pretreated in a N_2 flow at 500°C.

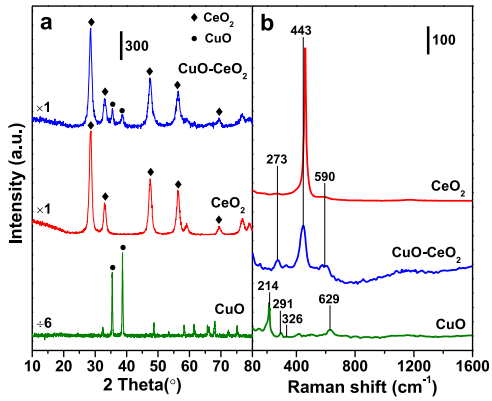

Fig. 1. XRD patterns (a) and Raman spectra (b) of the catalysts.

2.3. CO self-sustained catalytic combustion

The catalytic activity was evaluated in a flow-type apparatus designed for continuous operation. A powdered catalyst (weight 200 mg, particle size 0.1–0.15 mm) was packed into a quartz tube reactor with an inner diameter of 4 mm. The flow rates of CO, O_2 and N_2 (0.2 L/min) were controlled by mass flow controllers with a full-scale measurement accuracy of ±1%. Temperature-programmed catalytic ignition of CO was performed at a heating rate of 5°C/min, and two K-type thermocouples (0.5 mm thick) were used. The first thermocouple was located in front of the catalyst bed to control the oven temperature along the flow; the second thermocouple was inserted into the center of the catalyst bed to continuously monitor the temperature. Effluent gas was analyzed using an online multicomponent analyzer (QGS-08C for CO/CO_2 and OGS-10T for O_2, Maihak).

3. Results and discussion

3.1. Structural characterization

Fig. 1a shows the XRD patterns of the CuO, CeO_2 and CuO–CeO_2 catalysts. For CuO, the two sharp diffraction peaks at 35.6° and 38.8° are associated with (−111) and (111) planes in the monoclinic crystal structure (JCPDS 45-0937). Typical diffraction peaks of CeO_2 are observed at 28.6°, 33.1°, 47.5° and 56.4°, which correspond to the (111), (200), (220) and (311) planes, respectively with fluorite structures (JCPDS 34-0394). Similar diffraction peaks can be observed in the CuO–CeO_2 catalyst, with a lower intensity than that of CeO_2. The weak diffraction peaks of CuO indicate that either a $CuCeO_x$ solid solution is formed or dispersed CuO clusters anchor onto the ceria surface. The Raman spectrum of CuO (Fig. 1b) also

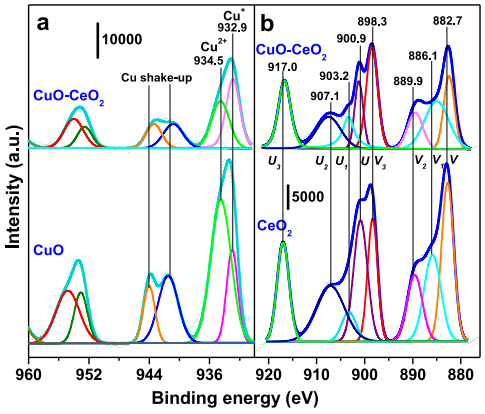

Fig. 2. XPS narrow spectra of Cu 2p (a) and Ce 3d (b) (Ce^{3+}: v_1 *and* u_1, Ce^{4+}: *v*, v_2, v_3, *u*, u_2 and u_3) over the catalysts.

reveals a monoclinic cupric oxide phase, according to the A_{1g}, B_{1g} and B_{2g} modes located at 291, 326, and 629 cm^{-1}, respectively, but the peak at 214 cm^{-1} demonstrates the existence of Cu_2O [12]. The spectrum of CuO–CeO_2 catalysts shows a main band at approximately 443 cm^{-1}, which is related to the F_{2g} symmetry vibration mode of the cubic fluorite structure of CeO_2. Notably, the position of the F_{2g} band deviates from that of pure CeO_2 (460 cm^{-1}) since the incorporated copper ions induce a lattice distortion of CeO_2, which influences the polarizability of the symmetrical stretching mode of the [Ce-O_8] vibrational unit [13]. The formation of surface oxygen vacancies is confirmed by two weak peaks at approximately 273 and 590 cm^{-1}. According to the ratio of the two peak areas at 590 and 443 cm^{-1} (A_{590}/A_{443}), the concentration of surface vacancies is analyzed semiquantitatively for these catalysts, following the order of CuO–CeO_2 (0.36) > CeO_2 (0.02) > CuO (0.00).

The chemical states and surface compositions of the catalysts are investigated by XPS, detecting under the vacuum pressure (1×10^{-7} Torr) rather than ambient pressure is employed to obtain valence states during heating process at the H_2 atmosphere [14]. Before the test, the samples were vacuumized to remove the moisture until the vacuum reached 5.0×10^{-9} mbar in the analyzer chamber. For the binding energy of Cu 2p (Fig. 2a), the presence of the shake-up peak at 938-947 eV and the lower Cu $2p_{3/2}$ binding energy appearing at 932.9 eV are two major XPS characteristics of Cu^{2+} and Cu^+, clearly suggesting the Cu^{2+}/Cu^+ redox pair exists in both CuO and CuO–CeO_2 catalysts. Fig. 2b shows the deconvoluted spectra of Ce 3d, which is decomposed into four pairs of spin-orbital doublets labeled as *v* and *u*, corresponding to $3d_{3/2}$ and $3d_{5/2}$, respectively. The peaks labeled as *v*, v_2 and v_3 correspond to the $3d_{3/2}$ level of Ce^{4+},

Table 1
Surface compositions and H_2 consumption of the catalysts.

Catalyst	Surface atomic ratio		H_2 consumption (mmol/g)
	Cu^+/Cu^{2+}	Ce^{3+}/Ce^{4+}	
CuO	0.46	/	7.28
CeO_2	/	0.21	0.46
CuO–CeO_2	1.25	0.35	2.81

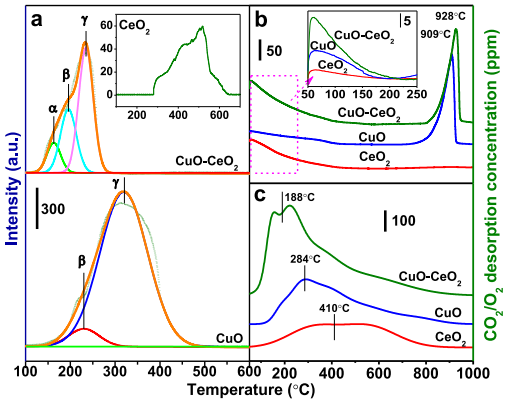

Fig. 3. H_2-TPR-TCD (a), O_2-TPD-MS (b) and CO-TPD-MS (c) profiles of the catalysts.

while the peaks tagged as *u*, u_2 and u_3 are assigned to the $3d_{5/2}$ of the Ce^{4+}. The couple v_1-u_1 is considered the fingerprint of Ce^{3+} species that favors the formation of oxygen vacancies on the catalyst surface. The surface Cu and Ce components, determined by integrating the areas of Cu 2p and Ce 3d peaks, as shown in Table 1. The Cu^+/Cu^{2+} was calculated by the ratio of relative area of Cu^+ peak to the Cu^{2+} peak. The Ce^{3+}/Ce^{4+} was obtained by the ratio of the total area of the Ce^{3+} peaks to the Ce^{4+} region. According to the surface compositions of the copper and cerium species listed in Table 1, the Cu^+/Cu^{2+} and Ce^{3+}/Ce^{4+} ratios of CuO–CeO_2 are higher than those of bulk CuO and CeO_2, respectively, indicating that these Cu^+ species are produced on the Cu^+-[O_v]-Ce^{3+} interface ([O_v]= surface oxygen vacancy) via Ce^{4+} reduction to form Ce^{3+}.

3.2. Temperature-programmed analysis of the catalysts

The redox behavior of the catalysts was investigated by H_2-TPR. A faint reduction of pure CeO_2 is observed at temperatures > 280°C (Fig. 3a), arising from the poor redox properties of the ceria species. The reduction of the CuO catalyst initiates at surficially dispersed CuO_x clusters centered at 230°C (β peak), but a broad peak at 319°C (γ peak) dominates, which corresponds to the reduction of

bulk CuO. The H_2-TPR profile of the CuO–CeO_2 catalyst is characterized by three partially overlapping peaks at 163 (α peak), 196 (β peak) and 235°C (γ peak), which are attributed to the reduction of copper species in the $CuCeO_x$ solid solution, dispersed CuO_x clusters and crystallized CuO, respectively. It is evident that the synergistic effect of the interaction between CuO and CeO_2 results in lower reduction temperatures compared to those of the pure materials. Although the H_2 consumption of CuO–CeO_2 (2.81 mmol•g^{-1}, Table 1) is lower than that of CuO (7.28 mmol•g^{-1}), the catalytic activity test, which will be discussed in the subsequent section, confirms that the redox properties of the catalysts decrease mainly according to their reduction temperature rather than H_2 consumption, following the sequence CuO–CeO_2 > CuO > CeO_2.

O_2-TPD is used to investigate the mobility of oxygen species in all catalysts. As shown in Fig. 3b, all the catalysts display desorption peaks centered at 59°C, assigned to the desorption of physisorbed oxygen (O_{ads}). Clearly, the CuO–CeO_2 exhibits a stronger O_{ads} peak, followed by CuO and then CeO_2. These results suggest that the abundant active oxygen connects with oxygen vacancies (Cu^+-[O_v]-Ce^{3+}) that are easily released from the CuO–CeO_2 surface to participate in the oxidation reaction. Pure CuO is a nonstoichiometric oxide, as confirmed by XPS, where the cation deficiency formed tends to adsorb oxygen more easily than CeO_2. Therefore, the contribution of vacancies (Ce^{4+}-[O_v]-Ce^{3+}) over pure CeO_2 to oxygen adsorption is quite limited. The desorption peak of CuO at 909°C corresponds to lattice oxygen (O_{lat}) escaping from copper cations. Because CeO_2 is thermally stable, it has no lattice oxygen desorption. The synergistic effect between copper and cerium leads to a shifting of the O_{lat} peak to a higher temperature (928°C) and the intensity weakening of the CuO–CeO_2. Compared with CeO_2 and CuO–CeO_2, CuO exhibits the high mobility of O_{lat}, which might accelerate the oxygen transfer from the bulk to the surface, favoring a reaction at high temperatures.

The CO-TPD results over the catalysts are shown in Fig. 3c. In a comparison of the three catalysts, the CuO–CeO_2 catalyst reveals that CO desorbed at the lowest temperature with highest intensity, followed by CuO and lastly CeO_2. All CO molecules adsorbed on the catalyst surface desorbed as CO_2 during the heating cycle with no remaining CO signal detected. This finding indicates that lattice oxygen is involved in CO oxidation and that the amount of desorbed CO_2 reveals the quantity of the active surface lattice oxygen on the catalyst. The O_2-TPD experiments show that the CuO and CuO–CeO_2 catalyst gives the O_{lat} desorption signal at a temperature > 900°C, suggesting that the thermal depletion of O_{lat} is difficult. However, it should be noted that the depletion of O_{lat} can be much easier when a strong reducing agent (i.e., CO and H_2 shown in H_2-TPR) is present, particularly at the metal-support interface [15]. The involvement of O_{lat} in the reaction will be further discussed based on the kinetic results in the subsequent section.

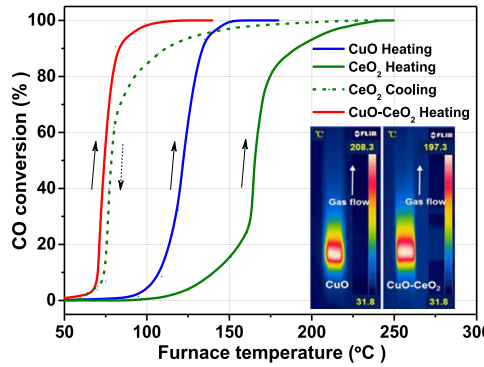

Fig. 4. Ignition curves of CO and the temperature fields in the reactor under a 5% CO+10% O_2/N_2 atmosphere.

3.3. Temperature-programmed catalytic ignition of CO

The catalytic combustor can exhibit a steady-state multiplicity typical of highly exothermic reactions, where increasing the temperature induces the transition of CO combustion from the step kinetically controlled to that controlled by diffusion. As shown in Fig. 4, the CeO_2 catalyst is inactive in order to achieve self-sustained combustion. The experimental run is performed by first raising the furnace temperature from a low conversion condition up to an ignited condition (heating process). However, the temperature was subsequently decreased, leading to the progressive blow out of the reaction (cooling process). For the CuO and CuO–CeO_2 catalysts, the rate increases slowly as the temperature increases and then much more steeply at the light-off stage. Once ignition occurs, complete CO conversion can be maintained even when the controlled temperature falls to room temperature. The CuO–CeO_2 catalyst exhibits the higher low-temperature activity than that of CuO according to the ignition temperatures of 72 and 117°C (defined as the temperature at 30% CO conversion). From the temperature profiles during CO self-sustained combustion (Insert in Fig. 4), however, CuO provides enough copper sites to adsorb CO and thus obtains a higher hot zone temperature (208.3°C) than does CuO–CeO_2 (197.3°C).

Using the best catalyst, i.e., CuO–CeO_2, the transient behavior of CO ignition was carried out under 1%-7%CO+5%O_2/N_2 conditions. Fig. 5 shows that CO self-sustained combustion can be achieved at CO concentrations ≥2%. Notably, from a partially enlarged view, the CO conversion

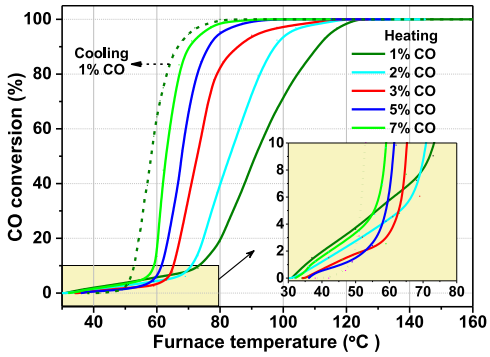

Fig. 5. Ignition curves of CO over the CuO–CeO_2 catalysts under a 1%-7%CO+5%O_2/N_2 atmosphere.

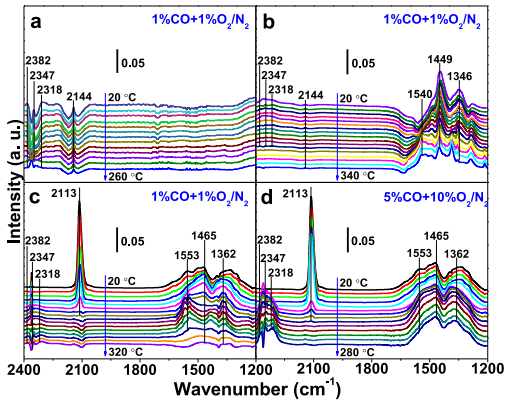

Fig. 6. In situ infrared spectroscopy analysis of CuO (a), CeO_2 (b) and CuO–CeO_2 (c and d) under 1%CO+1%O_2/N_2 and 5%CO+10%O_2/N_2 atmospheres, and the curves are listed by 20 °C intervals.

rate decreases during the induction process (CO conversion<10%) when the CO concentration increases from 1% to 5%. Such a slow reaction rate with high CO partial pressure is caused by the competitive coadsorption between CO and oxygen, where the kinetic transition occurs from an oxygen-covered surface to a CO-poisoned surface steady state that prevents the dissociation of O_2 [16]. This dilemma does not change significantly until it has entered the light-off stage with temperature. Once the accumulation of heat promotes ignition, the steady-state coverage of CO is diminished to the degree where the dissociation of O_2 can efficiently occur. Then, the adsorbed CO molecules react rapidly with oxygen to form CO_2. The light-off process has a high gas diffusivity $D_v \propto T^{1.81}$ and high mass transfer coefficient $K_s = (D_v \bullet S)^{1/2}$ (T denotes the temperature and S denotes the turnover frequency) [17], which leads to the retaliatory rise of the reaction rate (high slope, Fig. 5) with a CO partial pressure.

3.4. *In situ infrared spectroscopy analysis*

To further measure the intermediates of CO oxidation, in situ IR spectroscopy is used to monitor the adsorption and oxidation behavior of CO over the catalysts (Fig. 6). Gaseous CO is coordinated to the copper sites to form [Cu^+-CO] carbonyls on the CuO catalyst. Because the d-orbitals of the Cu^+ cations have an outer-shell electron distribution of 3d10, the synergy between the σ bonds and π-back-bonding is responsible for the catalyst stability [18]. Under a 1%CO+1%O_2/N_2 atmosphere, an increasing temperature leads to a decrease in the [Cu^+-CO] band, followed by the formation of CO_2. Here, the physically adsorbed CO_2 is observed in the ground vibrational state (2382 and 2347 cm^{-1}, P and R branches, respectively) and the transitions between the vibrationally excited states of the antisymmetric stretching mode (2318 cm^{-1}) [19]. Except for weak carbonyls formed on the CeO_2, CO tends to be chemisorbed at cerium sites to produce bidentate (1540 cm^{-1}) and monodentate carbonates (1449 and 1346 cm^{-1}), which decrease slowly with temperature, and thus, it is difficult to achieve CO_2 conversion [20]. A clear redshift of the carbonyl peak (2113 cm^{-1}) with a high intensity and a blueshift of carbonates are observed for CuO–CeO_2. The redshift might be induced by CO adsorption onto the oxygen vacancies at the interface between the copper and cerium oxides to form Cu^+-[C≡O]-Ce^{3+} species. Evidently, both π-back-bonding enhancement and σ-bond weakening determine this IR signal shifting, which strengthens the Cu-C bonds but decreases the C-O bond order, thus favoring CO oxidation. Therefore, under a 5%CO+10%O_2/N_2 atmosphere, Cu^+-[C≡O]-Ce^{3+} is a major contributor to CO ignition compared with the carbonates and immediately reacts with active oxygen to produce CO_2 at temperatures >100°C. The IR peak intensity of CuO–CeO_2 catalyst under the 1%CO+1%O_2/N_2 and 5%CO+10%O_2/N_2 was calculated in Fig. S5, suggesting that the CO-poisoned process occurs at low-temperature (20-100°C) for 5%CO, in keeping with the kinetically limited regime data in Fig. 5 although existing the difference reaction conditions between IR experiments and activity tests.

3.5. *Kinetic model of CO catalytic ignition*

3.5.1. *Steady state transformation induced by step-response runs*

The catalytic ignition process represents a convolution of the reaction kinetics and heat generation since the heat produced is governed by the reaction rate that in turn is determined by the reaction kinetics. However, the temperature triggers a kinetic transition from a low-rate steady-state regime to a high-rate steady-state regime, which should be well distinguished before the ki-

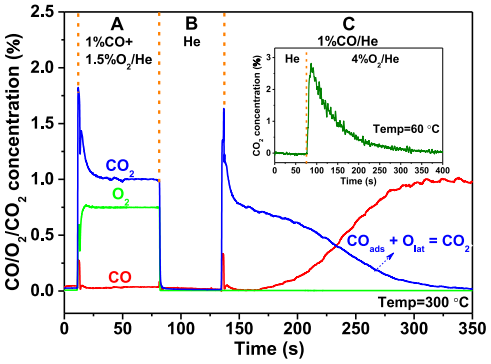

Fig. 7. Isothermal oxidation of CO over the CuO–CeO_2 catalyst.

netic model of the CO catalytic ignition is established. During the induction process, the reactivity of the adsorbed [Cu^+-(C≡O)-Ce^{3+}] species with adsorbed oxygen species (O_{ads}) was investigated by transient response runs at 60°C, as presented in the insert of Fig. 7. After CO saturation in 1 h, 5%CO/He (100 mL/min) was removed from the feed flow, while the catalyst was continuously flushed with helium until the baseline was stable. A switch to He→4%O_2/He permitted the oxidation of the Cu^+-[C≡O]-Ce^{3+} species for a duration of O_2, where the molar fraction of CO_2 increased and passed through a maximum. No CO signal was detected during the isothermal oxidation process, indicating that CO adsorption to form Cu^+-[C≡O]-Ce^{3+} dominated over O_2 adsorption.

It has been previously shown that there is a large amount of lattice oxygen (O_{lat}) on the surface of the CuO phase that contributes to the self-sustained catalytic combustion of CO, which was confirmed by the transient response run in Fig. 7. In Part A, 1%CO+1.5%O_2/He was fed to the reactor at 300°C, where the reaction involving sufficient O_2 and CO led to 100% CO conversion. The CO_2 signal started at a sharp step-response and then decreased with time until a steady state was achieved. Then, after purging in helium (Part B) to remove the gas phase, a 1%CO/He mixture was introduced into the reactor (Part C). Following another step-response of the CO_2 signal, which deceased with time, the CO outlet concentration showed a dead time, i.e., a period during which the fed CO reacted with O_{lat} of the surface CuO, then it increased with time, approaching the inlet value of 1% until all the O_{lat} was completely consumed.

3.5.2. *Determination of the kinetic parameters*

Based on the CuO–CeO_2 catalyst, the kinetics of CO oxidation during the induction process was simulated according to the reaction involving adsorbed CO and O_2 molecules under a 5%CO+10%O_2/N_2 (P_{CO}=5050 Pa, P_{O2}=10100 Pa) atmosphere. Considering CO adsorption as the rate-determining step of the oxidation, the CO adsorption, desorption and reaction steps are assumed at equilibrium. Hence, the kinetic relationships during the induction process can be written (M_i) [21] as

$$k_{ac}P_c(1-\theta_c) - k_{dc}\theta_c - k_{r1}\theta_{oa}\theta_c = 0 \quad (1)$$

where θ_c and θ_{oa} denote the CO and O coverage arising from adsorbed CO and O_2, respectively; and P_c, k_{ac}, k_{dc} and k_{r1} are the partial pressures of CO, the rate constants of CO adsorption and desorption, and the CO+O surface reaction during the induction process, respectively. The exact solution of Eq. 1 is

$$\theta_c = \frac{K_c P_c}{1 + K_c P_c + (k_{r1}/k_{dc})\theta_{oa}} \quad (2)$$

K_c=k_{ac}/k_{dc} is the adsorption coefficient of CO. Because the surface is primarily covered by CO during the induction process and a low reaction rate is observed at relatively high CO pressure, the O coverage (θ_{oa}) according to Langmuir's model [22] can be approximated as

$$\theta_{oa} = \frac{(K_{oa}P_{oa})^{0.5}}{1 + (K_{oa}P_{oa})^{0.5}} \approx (K_{oa}P_{oa})^{0.5} \quad (3)$$

where K_{oa} is the adsorption coefficient of O_2. Then, the reaction rate r_1 is calculated as follows:

$$r_1 = k_{r1}\theta_c\theta_{oa} \quad (4)$$

The catalytic ignition of CO reflects the switching from a low-reactivity metallic surface to a high-reactivity oxide surface; thus, the surface is mainly covered by oxygen during the self-sustained combustion stage. Considering the dissociation of oxygen, the rate equations during self-sustained combustion can be established based on the conservation of adsorbed CO and O_{lat} species, (M_s):

$$K_c P_c(1-\theta_c) - \theta_c - \left(\frac{k_{r2}}{k_{dc}}\right)\theta_c\theta_{ol} = 0 \quad (5)$$

$$K_{ol}P_o(1-\theta_{ol})^2 - \theta_{ol}{}^2 - (k_{r2}/k_{dol})\theta_{ol}\theta_c = 0 \quad (6)$$

where θ_{ol} and k_{r2} denote the O coverage and the rate constants during CO self-sustained combustion, respectively. The relevant kinetic parameters mentioned above are determined in the supplementary information, with the description of kinetic models, as illustrated in Fig. 8. Due to the self-poisoning of CO on the surface, the induction step is depicted as a slow process, and both adsorbed CO and adsorbed O_2 participate in the oxidation reaction. The θ_c decreases at a relatively slow rate to 0.98 until an ignition temperature of 72°C (M_i), followed by the rate of CO oxidation r_1 increasing to 1.1×10^4 s^{-1}. The catalytic ignition of CO leads to an abrupt decrease in θ_c from 0.98 at 72°C (M_i) to 0.006 at 197°C (M_s) (see Section 3.3), which is associated with a high CO conversion. The rate

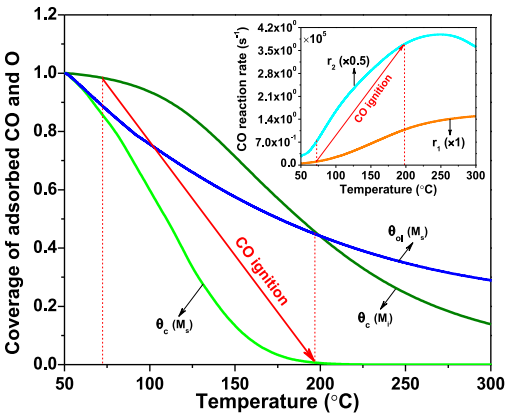

Fig. 8. Coverage of adsorbed CO and O as well as rates of CO oxidation in the induction and self-sustained combustion processes.

of CO oxidation r_2 (7.4×10^5 s^{-1}, M_s) in the self-sustained combustion process is much higher than that (r_1) during the induction process (1.1×10^4 s^{-1}, M_i). It is inevitable that the partially active O_{lat} species of CuO contribute to CO oxidation, corresponding to θ_o decreasing to 0.44 at 197°C. However, the created oxygen vacancies are immediately replenished by the dissociation of gaseous O_2 on the catalyst surface. According to the changes of bed temperatures, the ignition curve of CuO–CeO_2 catalyst is well reproduced by the kinetic model and shown in Fig. S6. Hence detailed reaction mechanism are as follows: CO is preferentially adsorbed on Cu^+-[O_v]-Ce^{3+} to yield carbonyls in induction process, which interact with adsorbed oxygen at vacancies to form CO_2; CO adsorbed and reacted on cerium sites (carbonates) provides faint contribution to CO ignition. Entering the ignition process, the fast heat/mass transport leads to the carbonyls reacted with lattice oxygen of CuO, followed by a thermochemical runaway.

4. Conclusion

CuO, CeO_2 and CuO–CeO_2 catalysts were prepared to investigate the contribution of active sites over the CuO–CeO_2 to CO ignition. The activity test demonstrated that CeO_2 is inactive for the ignition of CO. The CuO–CeO_2 catalyst ignition temperature of 72°C exhibits a higher low-temperature activity than that of CuO corresponding to the ignition temperature of 117°C. However, CuO provided enough copper sites to adsorb CO and abundant active lattice oxygen, and thus showed a higher hot zone temperature than that of CuO–CeO_2. During the induction process, the oxygen vacancies (Cu^+-[O_v]-Ce^{3+}) were analyzed by Raman, XPS, CO-TPD and in situ IR spectroscopy techniques and were the adsorption sites for the adsorption and activation of CO molecules. CO adsorption on the Cu^+-[O_v]-Ce^{3+} sites dominated over O_2 adsorption, i.e., self-poisoning of CO. The formed Cu^+-[C≡O]-Ce^{3+} species is a major contributor to CO ignition but results in a relative rate until entering the light-off stage as a function of temperature. Based on step-response runs and kinetic models, the kinetic phase transition, from a Cu^+ surface mainly covered by CO to that mainly covered by active lattice oxygen, occurs after the catalytic ignition, where the rate of CO oxidation during the self-sustained combustion process is much higher than that during the induction process. Although partially active lattice oxygen of CuO participates in CO oxidation, the oxygen vacancies created are immediately replenished by the dissociation of gaseous O_2 on the catalyst surface.

Declaration of Competing Interest

The authors declare that they have no known competing financial interests or personal relationships that could have appeared to influence the work reported in this paper.

Acknowledgments

We gratefully acknowledge the financial support from the National Natural Science Foundation of China (No. 51776216 and 51736010) and the Strategic Priority Research Program of the Chinese Academy of Sciences (No. XDA21040500).

Supplementary materials

Supplementary material associated with this article can be found, in the online version, at doi: 10.1016/j.proci.2020.06.186.

References

[1] Y. Deng, T. Wang, L. Zhu, A.P. Jia, J.Q. Lu, M.F. Luo, *Appl. Surf. Sci.* 442 (2018) 613–621.
[2] F. Bin, X.L. Wei, Bo Li, K.S. Hui, *Appl. Catal. B: Environ.* 162 (2015) 282–288.
[3] M. Konsolakis, *Appl. Catal. B: Environ.* 198 (2016) 49–66.
[4] G. Avgouropoulos, T. Ioannides, *Appl. Catal. A: Gen* 244 (2003) 155–167.
[5] G. Avgouropoulos, T. Ioannides, H.K. Matralis, *Appl. Catal. B: Environ* 56 (2005) 87–93.
[6] G. Avgouropoulos, T. Ioannides, H.K. Matralis, J. Batista, S. Hocevar, *Catal. Lett* 73 (2001) 33–40.
[7] D. Gamarra, G. Munuera, A.B. Hungría, M. Fernández-García, J.C. Conesa, P.A. Midgley, X.Q. Wang, J.C. Hanson, J.A. Rodríguez, A. Martínez-Arias, . *Phys. Chem. C* 111 (2007) 11026–11038.

[8] J. Lu, J. Wang, Q. Zou, D. He, L. Zhang, Z. Xu, S. He, Y. Luo, *ACS Catal* 9 (2019) 2177–2195.
[9] K. Mudiyanselage, et al., *Angew. Chem. Int. Ed.* 52 (2013) 5101–5105.
[10] R.N. Kang, X.L. Wei, P.D. Ma, F. Bin, J.Y. He, Q.L. Hao, B.J. Dou, *Fuel* 263 (2020), doi:10.1016/j.fuel.2019.116637.
[11] R.N. Kang, X.L. Wei, F. Bin, Z.B. Wang, Q.L. Hao, B.J. Dou, *Appl. Catal. A, Gen* 565 (2018) 46–58.
[12] D. Powell, A. Compaan, J.R. Macdonald, R.A. Forman, *Phys. Rev. B.* 12 (1975) 20–25.
[13] P.N. Amaniampong, Q.T. Trinh, K. Li, S.H. Mushrif, Y. Hao, Y. Yang, *Catal. Today* 306 (2018) 172–182.
[14] E.B. Fox, A.F. Lee, K. Wilson, C.S. Song, *Top. Catal* 49 (2008) 89–96.
[15] A. Chen, X. Yu, Y. Zhou, et al., *Nature Catal* 2 (2019) 334–341.
[16] V.P. Zhdanov, *J. Chem. Phy.* 126 (2007) 074706.
[17] W.L. Mccabe, J.C. Smith, Peter Harriott, *Chem. Eng. Unit Oper.* 4 (1993) 527–565.
[18] K.I. Hadjiivanov, M.M. Kantcheva, D.G. Klissurski, *J. Chem. Soc., Faraday Trans.* 92 (1996) 4595–4600.
[19] M.J. Pollard, B.A. Weinstock, T.E. Bitterwolf, P.R. Griffiths, A.P. Newbery, J.B. Paine, *J. Catal.* 254 (2008) 218–225.
[20] F. Bin, R. Kang, X. Wei, Q. Hao, B. Dou, *Proc. Combust. Inst.* 37 (2019) 5507–5515.
[21] A. Bourane, D. Bianchi, *J. Catal.* 222 (2004) 499–510.
[22] J. Nordstrand, J. Dutta, *J. Phys. Chem. C* 123 (2019) 16479–16485.